An Ultrasonically Powered and Controlled Ultra-High-Frequency Biphasic Electrical Neurostimulator

Lucia Tacchetti[1], Wouter A. Serdijn[1], Vasiliki Giagka[1,2]
[1]*Section Bioelectronics, Dept. Microelectronics, Faculty EEMCS, Delft University of Technology, Delft, The Netherlands*
[2]*Technologies for Bioelectronics Group, Fraunhofer Institute for Reliability and Microintegration IZM, Berlin, Germany*
taclucia@gmail.com, W.A.Serdijn@tudelft.nl, V.Giagka@tudelft.nl

***Abstract*—This paper presents the design of a neurostimulator performing biphasic ultra-high-frequency electrical stimulation while being driven from ultrasound energy. Unlike conventional constant current or constant voltage stimulators or state-of-the-art ultra-high-frequency stimulators, the system does not convert the input AC signal into regulated DC for storing power and supplying the elements of the circuits. Instead, it uses the received ultrasonic signal frequency (≥1 MHz) for electrically stimulating the tissue directly, and it achieves biphasic stimulation with external control and without storing extra power. This results in a highly efficient and miniature circuit, which has the potential to be used in bioelectronic medicine for stimulating small peripheral nerves deep inside the body. The operation of the circuit was first simulated in LTSpice using a lumped elements model for the impedance of the piezoelectric receivers and the load. Finally, a prototype was tested in vitro with commercial transducers and platinum-iridium electrodes as load.**

Keywords*—*ultrasound, neurostimulator, biphasic electrical stimulation, ultra-high-frequency stimulation, bioelectronic medicine

I. Introduction

Implantable neurostimulators have been employed over the past few decades, paving the way towards bioelectronic medicine. Programmed therapeutic electrical stimulation patterns are applied to the human neural pathways to address conditions such as Parkinson's disease, chronic pain, epilepsy, migraine and bladder dysfunction. The goal is to induce or inhibit action potentials travelling throughout the body, in order to modulate the operation of an organ and/or muscles [1],[2].

Generally, neurostimulators can be powered from an external source that wirelessly delivers energy to the implant to either recharge a battery or directly supply the electronics [3]. In such a scenario, the received AC signal is rectified, stored and regulated to supply the usually low-voltage blocks of the rest of the system. Nonetheless, up-conversion by means of a boost converter is often required to provide enough voltage compliance to operate an output stage connected to the stimulating electrodes as in Fig. 1(a) [4],[5].

Conventionally, biphasic constant current (CC) or constant voltage (CV) pulses are selected for stimulating nerve tissue. The first (usually cathodic) phase has the purpose of activating the excitable nerve fibers, while the second (usually anodic) phase reverses the direction of the stimulation current to avoid long-term accumulation of charge that might damage the electrodes and/or tissue [6].

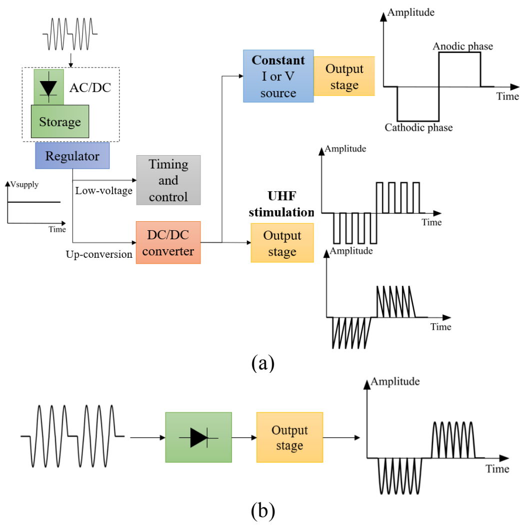

Fig. 1. General blocks scheme and shape of stimulating pulses for (a) a constant current/voltage stimulator or for a conventional UHF stimulator, and for (b) proposed UHF stimulator.

Alternatively, ultra-high-frequency (UHF) stimulation can be employed. This consists of current or voltage pulses at a high frequency (≥1 MHz) that are integrated by the capacitive nature of the axon membrane, thus leading to a 'staircase' increase of the membrane potential and, eventually, activation of the fiber [7]. The UHF pulses can be obtained from a DC source and the operation of high-frequency switches as in Fig. 1(a). Such pulses can be of different shapes: for example, rectangular or triangular pulses. The latter waveform is the output of the neurostimulator reported in [8], in which the authors showed an improved power efficiency in multichannel operation when compared to conventional CC stimulators. Moreover, they reduced the number of external components to only one inductor for generating the 1 MHz stimulating pulses.

Taking a more radical approach, it is possible to avoid the lossy conversion from AC to regulated DC and from that to high-frequency stimulation by eliminating the need for power storage, regulation and up-conversion. To this end, we propose to generate UHF pulses by rectifying the sinusoid obtained from an ultrasound transducer and using the obtained waveform to directly stimulate the tissue in a biphasic fashion as in Fig. 1(b).

The interest in ultrasonic waves as source of power and data for implantable medical devices (IMDs) has recently grown, particularly due to the advantages over RF and inductive coupling power transfer. In fact, ultrasound can deliver higher power to mm-sized and deeply (>10 cm) implanted receivers than the other techniques. Moreover, acoustic waves do not interfere with electromagnetic fields [9].

Implanted CC nerve stimulators powered from ultrasound are presented in [10] and [11]; the AC signal from a piezoelectric transducer is converted into DC to store power in an external capacitor and supply an integrated circuit. To date, only one device uses electrical pulses from a piezocrystal for directly stimulating the tissue [12]. The authors were able to stimulate the sciatic nerve of a rat with one pair of electrodes driven by their system. However, the stimulator is only capable of monophasic stimulation, which would quickly damage the electrodes and/or tissue. Furthermore, it allows for only half-wave rectification of the incoming signal, and a DC-blocking capacitor is included in the architecture for passive charge balancing. This could lead to an unwanted voltage offset generated across the electrodes after stimulation [13].

Therefore, in this paper, we propose a novel neurostimulator architecture that, by harvesting ultrasonic waves, is capable of electrical biphasic UHF stimulation without the need of power storage and internal control.

This paper is structured as follows: Section II explains the architecture and working principle of the proposed system. Section III describes the electrical models used in simulations for the piezoelectric receivers and the load, and illustrates the setup employed in measurements. The results of both simulations and measurements are shown in Section IV. Finally, Section V discusses these results and concludes the paper.

II. Proposed System

The concept of the proposed system for UHF biphasic neural stimulation is shown in Fig. 2. Two piezoelectric elements of different dimensions are used to receive ultrasonic waves and convert them into high-frequency electrical pulses that are delivered towards a pair of electrodes. The choice of two piezo elements has the aim of providing biphasic stimulation without the need of a separated unit to control and power the switches. The required phase of the pulse (i.e., cathodic or anodic) is selected by sending ultrasound at the specific resonant frequency of the corresponding piezo.

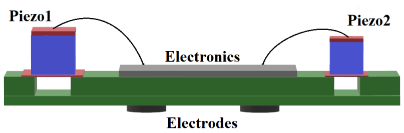

Fig. 2. Conceptual design of the system for UHF biphasic electrical stimulation with ultrasound piezoelectric receivers.

The electronics of the system consist of two bridge rectifiers for full-wave rectification of the received signal and two p-channel MOSFETs, M_1 and M_2, connected as in Fig. 3. When piezo P_1 is vibrating at its resonant frequency, the incoming signal is rectified and M_1 switches on, allowing current to flow from node A (anode, in this case) to node C (cathode, in this case), while M_2 is off, thus avoiding current flowing towards the other bridge. Similarly, when piezo P_2 is vibrating at its resonant frequency, M_2 turns on, while M_1 switches off, and current flows from node C to node A.

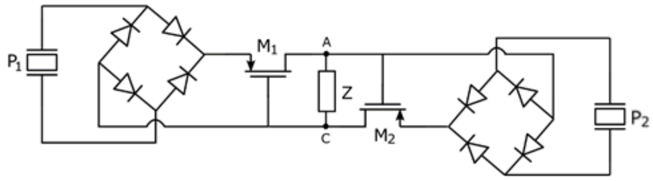

Fig. 3. Schematic of the proposed topology.

III. Models and Setup

A. Model of Piezoelectric Receiver and Load Impedance

When operating around resonance, the piezoelectric ultrasound receiver can be modelled with lumped elements as in Fig. 4 [14]. For matched source and load impedances, the peak amplitude of the open-circuit voltage developing across the piezo receiver is found to be [15]:

$$V_{oc} = \sqrt{8 \times \eta_{pc} \times I_{acou} \times A \times R_p} \quad (1)$$

where η_{pc} indicates the power-conversion efficiency of the transducer, A its surface area, R_p the resistance of the piezo at short-circuit resonance, and I_{acou} the transmitted acoustic intensity, which should not exceed 7.2 mW/mm^2, as defined by the FDA for the use of diagnostic ultrasound [16].

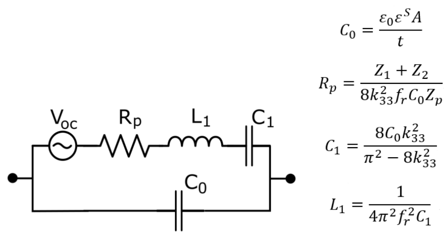

Fig. 4. Model of the electrical impedance of a piezoelectric receiver with equations for calculating the values of the passive elements.

For simulations, transducers made of PZT-5H with short-circuit resonant frequencies (f_r) 1 MHz and 2.6 MHz were modelled as in Fig. 4. Their thicknesses (t) and surface areas (A) are 1.05 mm, 0.41 mm and 1 mm^2, 0.16 mm^2, respectively. Material properties were taken from [14] and are reported in Table I. The acoustic impedances of the loads at the opposite piezo faces are Z_1=1.6 MRayls and Z_2=400 Rayls, representing tissue and air, respectively. Finally, each electrode at the load was modelled with a series connection of a resistor R_s, representing the electrolyte, and a capacitor C_{dl}, modelling the electrode-tissue interface [17]. Values for R_s and C_{dl} were assumed to vary in the range of 200 Ω - 2 kΩ and 100 nF - 10 µF, respectively [8].

TABLE I. PZT-5H Properties.

Relative dielectric constant (zero strain), ε^S	Piezoelectric coupling coefficient, k_{33}	Acoustic impedance (MRayls), Z_p
1470	0.75	29

B. Simulation and Measurement Setup

Circuit simulations were run in LTSpice using the electrical models for the impedance of the piezo elements and the load as previously described.

Piezoelectric transducers and a water tank for measurements were provided by the TUDelft Imaging Physics department. The transmitters were two Olimpus® half-inch immersion transducers working at 1 MHz and 2.25 MHz, respectively. The receivers were two disc-shaped piezoelectric elements mounted on a board for interfacing at the front with water through an acoustic transparent membrane, and at the back with air. In Fig. 5, the smaller element (P1) is 2 mm thick and has an impedance of around 200 Ω at 1 MHz, whereas the larger element (P2) has a thickness of 0.5 mm and an impedance of 12 Ω at 2.25 MHz. P1 and P2 were connected with wires to a PCB, also shown in Fig. 5 (top right).

An arbitrary waveform generator, followed by a power amplifier, was used to set the amplitude, frequency, duration, repetition rate, and delay of the sinusoidal bursts necessary to drive the ultrasonic transmitters. The measured signal was captured with an oscilloscope and plotted in MATLAB.

Finally, two platinum-iridium (PtIr) electrodes of 0.1 mm^2 from an array immersed in commercial phosphate buffered saline (PBS 0.01 M) were used as cathode and anode. Their impedance was measured to be about 4.2 kΩ at 1 kHz.

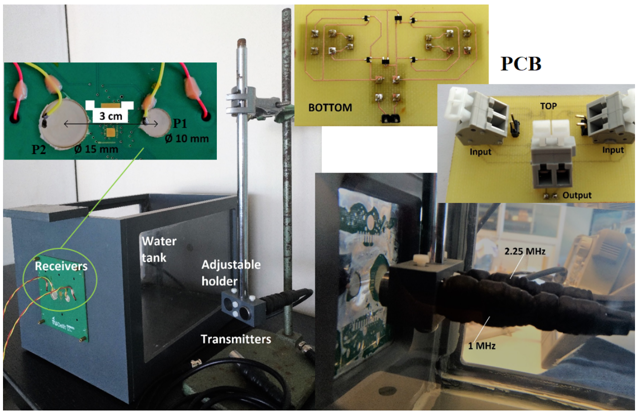

Fig. 5. On the left: setup with transducers and water tank. On the top-right: top and bottom sides of the fabricated PCB. On the bottom right: picture of the transmitters in water aligned at about 2 to 3 cm distance with the receivers on the other side of an acoustic transparent membrane.

IV. RESULTS

The voltage across the load was simulated in LTSpice for three different load impedances, each being the model of a series of two electrodes. V_{oc} (see Fig. 4) was set to 2 V peak for both phases. The resulting waveforms are plotted in Fig. 6 with a zoom of the cathodic and anodic pulses. The pulse width (PW) was 200 µs and 100 µs for the cathodic and anodic phase, respectively. The inter-phase delay (IPD) was set to 50 µs and the pulse repetition rate (PRR) to 100 Hz.

The power efficiency of the circuit is defined as the ratio between the power at the load (P_{out}) in between the two transistors and the power at the input of the rectifier (P_{in}). The latter is the product of the rms voltage seen at the input of the bridge and the current through it. P_{out}/P_{in} is plotted in Fig. 7, as a function of P_{in}, for different output resistive loads and two input signal frequencies. For these measurements, the input of the circuit was connected to a waveform generator producing a sinewave of controllable amplitude.

Both monophasic and biphasic stimulation were tested with the fabricated prototype. A monophasic 1 MHz burst was sent for 50 µs with a PRR of 10 Hz. The output voltage was measured across a series connection of 1120 Ω and 500 nF as load and can be seen in Fig. 8 with a detail of the high-frequency pulses. Biphasic stimulation was performed by sending a 1 MHz burst for the cathodic phase and a 2.25 MHz one for the anodic phase with an IPD of 50 µs. The PRR was 10 Hz and the PW 200 µs and 100 µs for the cathodic and anodic phase, respectively. The received open-circuit voltage is plotted in Fig. 9, while Fig. 10 shows (a) the voltage across the PtIr electrodes and (b) the current between them. The latter was obtained from the voltage recorded across a 1 kΩ resistor in series with the electrodes. At the end of the biphasic pulse, the output voltage presents a positive offset. This can be due to the imbalance in the injected charge during the two phases, or to the non-linearity of the electrode-electrolyte interface [13].

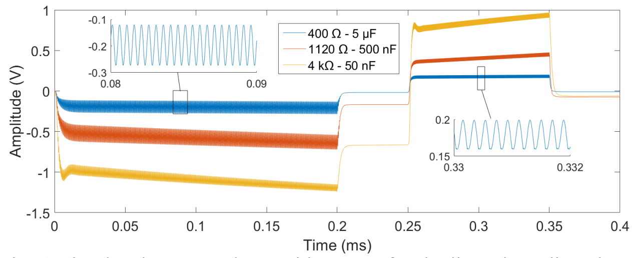

Fig. 6. Simulated output voltage with zoom of cathodic and anodic pulses.

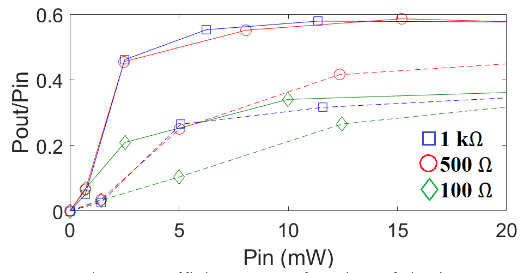

Fig. 7. Measured power efficiency as a function of the input power and for three different output loads. Solid lines are for a 1 MHz sinusoidal input, while the dashed lines are for a 2.6 MHz one.

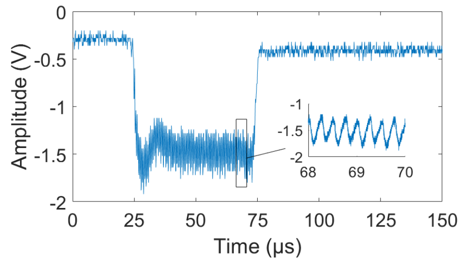

Fig. 8. Measured voltage across the load with a detail of the high-frequency pulses for a 1 MHz monophasic transmitted burst.

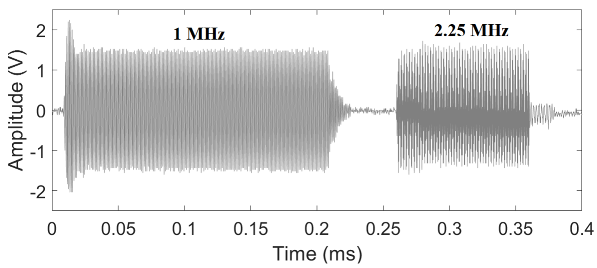

Fig. 9. Measured received 1 MHz and 2.25 MHz open-circuit voltage.

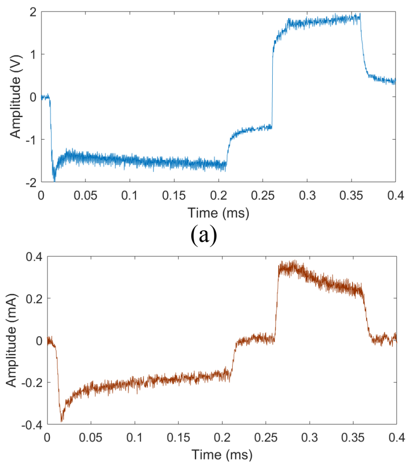

(a)

(b)

Fig. 10. Measured biphasic voltage (a) and current (b) between a pair of PtIr electrodes.

V. Discussion and Conclusions

Simulations showed the ability of the designed circuit to generate cathodic and anodic UHF pulses at the load from a sinusoidal input.

Measurements gave similar results concerning the shape of the waveform and confirmed that the proposed neurostimulator is capable of delivering UHF biphasic pulses when receiving a sinusoidal signal from ultrasound transducers and driving PtIr electrodes in PBS. The minimum amplitude of the input voltage V_{in} required for correct operation of the circuit was found to be around 2 V_{pp} for the selected diodes and pMOSTs. The maximum output voltage cannot exceed V_{in}-2V_d, V_d being the voltage drop of each diode.

The power efficiency of the circuit was found to be larger than 50 % for 500 Ω and 1 kΩ loads and for P_{in} larger than 5 mW with a 1 MHz input signal; this value decreases for higher frequencies and smaller load impedances. However, it could be improved with the selection of components having a lower voltage drop and higher operation speed. The link efficiency was not calculated due to the type of transducers used and limitations of the available setup; the receivers should be made smaller for implantation and designed to match the impedance of the circuit and load, thus maximizing the power transfer. A miniaturized prototype could then be realized to verify the operation *in vivo*. In particular, the total size of an implantable version of the device was estimated to be approximately 7 x 5.5 x 1.5 mm with the selected discrete components. However, this size may be reduced when choosing smaller elements and thus, could reach the dimensions of state-of-the-art ultrasonically powered neurostimulators (e.g., 6.5 x 3 x 2 mm as in [11]).

Future work will concentrate on the addition of extra stimulation channels and of real-time charge injection control so that the two phases could be regulated for delivering the same amount of charge. Furthermore, the effect of misalignment between the transmitters and the miniaturized receivers should be investigated. If one acoustic beam reaches both receivers, the two piezos, which should work at different phases, might instead give an output signal simultaneously, thus resulting in lower current though the load. This may be avoided with the use of focused transmitters and narrow-bandwidth receivers.

We demonstrated a circuit topology that, with low internal power losses and external control, provides UHF biphasic electrical pulses by harvesting ultrasound and has the potential to be used in a neurostimulator for targeting small peripheral nerves deep inside the body.

Acknowledgment

The authors would like to thank Verya Daeichin and Emile Noothout for providing the transducers setup, and Ali Kaichouhi for the help with the PCB fabrication and his technical advice during the project.

References

[1] K. Famm, B. Litt, K. J. Tracey, E. S. Boyden, and M. Slaoui, "A jump-start for electroceuticals," *Nature*, vol. 496, no. 7444, pp. 159–61, 2013.

[2] X. Li, W. A. Serdijn, W. Zheng, Y. Tian, and B. Zhang, "The injectable neurostimulator: an emerging therapeutic device," *Trends Biotechnol.*, vol. 33, no. 7, pp. 388–394, 2015.

[3] A. Ben Amar, A. B. Kouki, and H. Cao, "Power approaches for implantable medical devices," *Sensors*, vol. 15, no. 11, pp. 28889–28914, 2015.

[4] H.-M. Lee, H. Park, and M. Ghovanloo, "A power-efficient wireless system with adaptive supply control for deep brain stimulation," *IEEE J. Solid-State Circuits*, vol. 48, no. 9, pp. 2203–2216, 2013.

[5] V. Giagka, C. Eder, N. Donaldson, and A. Demosthenous, "An implantable versatile electrode-driving ASIC for chronic epidural stimulation in rats," *IEEE Trans. Biomed. Circuits Syst.*, vol. 9, no. 3, pp. 387–400, 2015.

[6] D. R. Merrill, M. Bikson, and J. G. R. Jefferys, "Electrical stimulation of excitable tissue: design of efficacious and safe protocols," *J. Neurosci. Methods*, vol. 141, no. 2, pp. 171–198, 2005.

[7] M. N. van Dongen, F. E. Hoebeek, S. K. E. Koekkoek, C. I. De Zeeuw, and W. A. Serdijn, "Efficacy of high frequency switched-mode stimulation in activating Purkinje cells," *arXiv:1406.7185v1 [q-bio.NC]*, 2014

[8] M. N. van Dongen and W. A. Serdijn, "A power-efficient multichannel neural stimulator using high-frequency pulsed excitation from an unfiltered dynamic supply," *IEEE Trans. Biomed. Circuits Syst.*, vol. 10, no. 1, pp. 61–71, 2016.

[9] H. Basaeri, D. B. Christensen, and S. Roundy, "A review of acoustic power transfer for bio-medical implants," *Smart Mater. Struct.*, vol. 25, no. 12, pp. 3001–3023, 2016.

[10] Y.-S. Luo *et al.*, "Ultrasonic power/data telemetry and neural stimulator with OOK-PM signaling," *IEEE Trans. Circuits Syst. II Express Briefs*, vol. 60, no. 12, pp. 827–831, 2013.

[11] J. Charthad *et al.*, "A mm-sized wireless implantable device for electrical stimulation of peripheral nerves," *IEEE Trans. Biomed. Circuits Syst.*, vol. 12, no. 2, pp. 257–270, 2018.

[12] P. J. Larson and B. C. Towe, "Miniature ultrasonically powered wireless nerve cuff stimulator," in Proc. *IEEE EMBS NER*, Cancun, Mexico, Apr. 2011, pp. 265–268.

[13] M. N. van Dongen and W. A. Serdijn, "Does a coupling capacitor enhance the charge balance during neural stimulation? An empirical study," *Med. Biol. Eng. Comput.*, vol. 54, no. 1, pp. 93–101, 2016.

[14] T. L. Szabo, *Diagnostic ultrasound imaging: inside out.* Hartford, Connecticut: Elsevier Academic Press, 2004.

[15] M. J. Weber, A. Bhat, T. C. Chang, J. Charthad, and A. Arbabian, "A miniaturized ultrasonically powered programmable optogenetic implant stimulator system," in Proc. *IEEE BioWireleSS*, Austin, TX, USA, Jan. 2016, pp. 12–14.

[16] *Information for manufacturers seeking marketing clearance of diagnostic ultrasound systems and transducers*, FDA. Rockville, MD, 2008.

[17] J. Malmivuo and R. Plonsey, "21. Functional electric stimulation," in *Bioelectromagnetism - Principles and Applications of Bioelectric and Biomagnetic Fields*, New York: Oxford University Press, 1995, pp. 493–508.